Interdiffusion at the Mn-CdTe(110) interface and the formation of metastable ternary semimagnetic semiconductor alloys

A. Wall
Department of Chemical Engineering and Materials Science, University of Minnesota, Minneapolis, Minnesota 55455 and IBM Corporation, Rochester, Minnesota 55901

A. Raisanen, G. Haugstad, L. Vanzetti, and A. Franciosi
Department of Chemical Engineering and Materials Science, University of Minnesota, Minneapolis, Minnesota 55455
(Received 13 August 1990; revised manuscript received 3 June 1991)

Mn vacuum deposition at room temperature onto CdTe(110) surfaces cleaved *in situ* yields atomic interdiffusion for metal coverages $\Theta \leq 3$ Å as a result of a partial Mn-Cd exchange reaction in the interface region. Synchrotron-radiation photoemission measurements show the reaction product to be a $Cd_{1-x}Mn_xTe$ semimagnetic semiconductor surface alloy. Large values of the average Mn concentration are achieved in such metastable interface reaction product. We use these results to explore the composition dependence of the electronic structure of ternary semimagnetic semiconductors.

I. INTRODUCTION

Ternary semimagnetic semiconductors[1-11] are substitutional alloys in which some of the group-II cations in a II-VI semiconductor are randomly replaced with magnetic impurities (usually Mn or Fe). In general, electronic parameters such as the energy gap E_g and the electron and hole mobilities of the semimagnetic ternaries exhibit a composition dependence similar to that observed in nonmagnetic ternary compounds. Furthermore, the presence of magnetic atoms produces a number of magneto-optical and magnetotransport phenomena unique to semimagnetic semiconductors, such as giant negative magnetoresistance, extremely large electronic g factors, and large Faraday rotation.[10,11]

The magnetic properties are the result of the exchange interaction between the magnetic moments localized on the Mn or Fe atoms and the band and impurity states.[10,11] The Mn magnetic moments mostly derive from the localized $3d$ orbitals, although studies have shown[5] that the Mn atomic configuration in $Cd_{1-x}Mn_xTe$ is $(d\uparrow)^5(s\uparrow)(p\uparrow)$ rather than $(d\uparrow)^5s^2$. Recent theoretical investigations[6-9,12,13] have therefore focused on the $3d$ contribution to the electronic structure of semimagnetic ternary semiconductors, and on the $3d$ hybridization with anion-derived p states. However, the spin polarization of the non-d orbitals also has a profound influence in determining the ternary electronic structure and the anomalous Curie temperatures of these materials and this has only recently been taken into account.[6]

The electronic structure of Mn-containing semimagnetic semiconductors has been the subject of recent systematic experimental investigations,[1,2] and probably no semimagnetic semiconductor has been studied experimentally and theoretically more than $Cd_{1-x}Mn_xTe$.[3-9] Since the Mn chalcogenides have different crystal structures as compared to the II-VI semiconductors, $Cd_{1-x}Mn_xTe$ can be produced in the form of single-phase bulk single crystals only for x up to 0.77.[10]

We present a synchrotron-radiation photoemission study of the interaction of Mn atoms with CdTe(110) surfaces at room temperature. Results for bulk $Cd_{1-x}Mn_xTe$ samples were also obtained for comparison. An investigation of the Cd $4d$, Te $4d$, and Mn $3d$ emission as a function of Mn coverage indicates that atomic interdiffusion across the interface results in Mn atoms partially replacing Cd atoms in the II-VI matrix to produce a $Cd_{1-x}Mn_xTe$ surface layer. Systematic studies as a function of the photoelectron escape depth indicate that the surface alloy composition is relatively homogeneous in the direction normal to the interface within the photoemission sampling depth. We used core photoemission results for the bulk ternary semimagnetic standards to calibrate the average composition $\bar{x}$ of the interface reaction product. We observed that the average composition increases with Mn coverage throughout the coverage range examined, corresponding to $0.15 \leq \bar{x} \leq 0.94$.[14]

Resonant photoemission studies of the Mn $3d$ contribution to the valence bands as a function of the average composition $\bar{x}$ revealed an unexpected composition dependence of the electronic structure of $Cd_{1-x}Mn_xTe$. Through this dependence we analyze here the origin of the previously reported many-electron satellite[4-6] and, in general, the relative importance of many-body effects and Mn d–Te p hybridization in determining the valence-band structure.

II. EXPERIMENTAL DETAILS

Single crystals of CdTe were cleaved *in situ* to expose mirrorlike atomically clean (110) surfaces. Mn deposition was performed from a resistively heated tungsten basket. The deposition rate was determined by means of a quartz microbalance. Thicknesses quoted in angstroms can be

converted to equivalent monolayers (ML's) using the CdTe(110) surface atomic density of 6.73×10^{14} atoms/cm^2 (1 ML=0.83 Å Mn). The system pressure during deposition was $<2\times10^{-10}$ Torr, and the spectrometer operating pressure was 2×10^{-11} Torr.

The experiments were performed at the Synchrotron Radiation Center at the University of Wisconsin–Madison. Radiation from the 1-GeV electron storage ring Aladdin was monochromatized with a 3-m toroidal-grating monochromator. Angle-integrated photoelectron energy-distribution curves (EDC's) were obtained with a commercial hemispherical electron-energy analyzer. The overall resolution (electrons plus photons) was estimated from the width of the Fermi-level cutoff in EDC's from thick unreacted metal films deposited on Si(111) samples *in situ*, and ranged from 0.2 to 0.45 eV for photon energies $40<h\nu<130$ eV. Radiation from a high-intensity tungsten lamp was focused through a viewport on the sample surface when necessary to eliminate electrostatic charging.

Bulk semimagnetic semiconductor samples of $Cd_{1-x}Mn_xTe$ ($x=0.20, 0.32, 0.45, 0.60, 0.68$) were grown at Purdue University through a modified Bridgmann method. X-ray diffraction showed the samples to be single-phase single crystals. The nominal Mn concentration (from the premelt constituents) was checked *a posteriori* with electron-microprobe analysis against calibrated standards. The samples were placed in the analysis chamber, cleaved *in situ* to expose (110) surfaces, and analyzed following the methodology described in Refs. 1–6.

III. RESULTS AND DISCUSSION

A. Interdiffusion at the Mn-CdTe(110) interface

We investigated the valence-band emission from the Mn-CdTe(110) interface through resonant photoemission[1–6] at the Mn $3p$-$3d$ resonance, and exploited the characteristic Mn $3d$ photoionization cross section to probe the Mn contribution to the valence emission. Electronic states which have Mn $3d$ character exhibit a minimum (antiresonance, $h\nu_{AR}\sim47$ eV) followed by a maximum (resonance, $h\nu_R\sim50$ eV) in the photoemission cross section as a function of photon energy.[1–6] This is the result of the quantum-mechanical interference of two possible photoexcitation channels: the direct excitation

$$3p^63d^54(sp)^2+h\nu\rightarrow3p^63d^44(sp)^2\epsilon f$$

and a Mn $3p$-$3d$ transition to a discrete excited state, followed by a super-Coster-Kronig decay,

$$3p^63d^54(sp)^2+h\nu\rightarrow3p^53d^64(sp)^2\rightarrow3p^63d^44(sp)^2\epsilon f\ .$$

The corresponding overall photoionization cross section can be calculated considering the interaction of the discrete excited state with the continuum through a formalism first discussed by Fano,[15] and then extended to transition metals by Davis and Feldkamp[16] and Yafet.[17]

Photoelectron energy-distribution curves of the valence-band emission from the interface as a function of Mn coverage Θ are presented in Fig. 1. For each coverage we show data at resonance ($h\nu_R=50$ eV, solid line) and antiresonance ($h\nu_{AR}=47$ eV, dashed line). The EDC's at resonance have been normalized to the photon flux and are plotted in relative units. The antiresonance EDC's (dashed line) are normalized to the integrated Cd $4d$ intensity of the corresponding resonance EDC at each Θ. The difference between EDC's taken at $h\nu_R$ and $h\nu_{AR}$ emphasizes the Mn $3d$ contribution.[6] Shown at the top of Fig. 1 for comparison is an EDC for a thick unreacted (50 Å) Mn film evaporated *in situ* on a Si(111) surface,[18] representative of unreacted metallic Mn emission. The binding energies are referred to the Fermi level E_F.

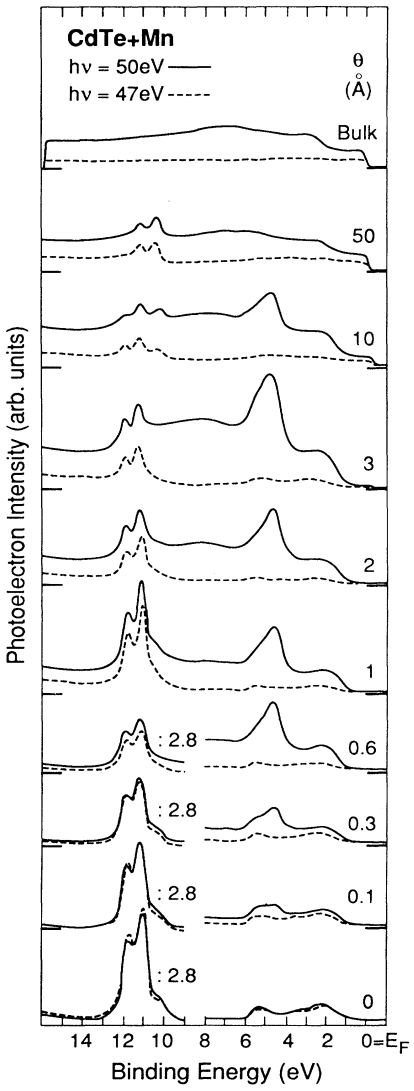

FIG. 1. Photoemission energy-distribution curves (EDC's) for the valence-band and shallow Cd $4d$ core-level emission during Mn-CdTe(110) interface formation at various coverages Θ (in Å). For each coverage we show EDC's for photon energies at the Mn $3d$-$3p$ resonance ($h\nu_R=50$ eV, solid line) and antiresonance ($h\nu_{AR}=47$ eV, dashed line). The difference emphasizes the Mn $3d$ contribution. The topmost EDC's were obtained for a thick unreacted Mn film on Si(111) (Ref. 18).

Prior to Mn deposition, the CdTe valence-band maximum E_v, estimated through a linear extrapolation of the leading valence-band edge, was found 0.75±0.10 eV below E_F.[19]

The two bottom-most spectra in Fig. 1 ($\Theta=0$ Å, solid and dashed lines) were obtained from CdTe(110) prior to metal deposition, and show that there are no major changes in the relative cross section of the binary-related electronic states between 47 and 50 eV of photon energy. Comparison with previous photoemission studies of CdTe,[20–22] and band-structure calculations,[7–9,23] indicate that a CdTe density-of-states (DOS) feature at 1–4 eV in Fig. 1 derives primarily from Te 5*p* states, while the feature centered at approximately 5 eV corresponds to Cd 5*s*–Te 5*p* hybrid states. The Cd 4*d* core-level emission appears 10–13 eV below E_F in Fig. 1. Analysis of the bulk CdTe electronic structure indicates that a valence-band feature with predominantly Te 5*s* character appears at approximately 10 eV (Refs. 19 and 24) as a low-binding-energy shoulder of the dominant Cd 4*d* doublet.

As Mn is deposited onto the CdTe(110), the antiresonance spectra ($h\nu_{AR}=47$ eV, dashed line) do not change significantly for $\Theta \leq 3$ Å, except for the progressive attenuation of the Cd 4*d* core emission. Large changes are visible, instead, in the resonance spectra (solid line) which emphasize the development of the Mn 3*d* contribution. Several Mn 3*d*–related features develop and grow with coverages for $0<\Theta\leq 3$ Å; they include a relatively sharp feature at 4.35 eV below E_F (or 3.60±0.10 eV below the linearly extrapolated valence-band edge), and two less intense features in the 1–3- and 7–9-eV range, respectively. Emission at E_F is not visible for $\Theta<3$ Å.

For $\Theta>3$ Å, a second stage in the evolution of the Mn 3*d* contribution emerges in Fig. 1. The emission at the Fermi level grows with the development of a sharp Fermi cutoff, the 4.35-eV major feature progressively disappears, and the overall Mn 3*d* line shape approaches that of bulk Mn. The Cd 4*d* emission is sharply attenuated, but some residual Cd 4*d* emission is visible, shifted to lower binding energies, even at the highest coverages examined (~50 Å).[25]

The position of E_F, as determined from the Fermi-level cutoff of the EDC's for 50-Å Mn films on CdTe(110), was found 0.25±0.10 eV to higher kinetic energy (lower binding energy) than that of Mn on Si(111), or a Cr film in electrical contact with the chamber. A similar effect (both in magnitude and polarity) was observed by John *et al.*[26] during a study of the Ag-CdTe(100) interface. John *et al.* proposed that the photoinduced rigid shift was due to a surface photovoltage[27–29] which compensated for an equilibrium potential difference of the metal surface relative to CdTe(110). Such a potential difference would be present (in the absence of illumination, and under equilibrium conditions) because of the low work function of the metal relative to CdTe(100). The same effect should be observed for Mn-CdTe(110), since the work-function difference for this system[20,30] is of the same sign and higher magnitude than that of Ag-CdTe(100).[26]

Analogous valence-band measurements were performed on bulk $Cd_{1-x}Mn_xTe$ samples (x=0.20, 0.32, 0.45, 0.60, and 0.68). Representative EDC's are shown in Fig. 2 for selected compositions, at photon energies near the Mn 3*p*-3*d* resonance ($h\nu_R=50$ eV, solid line) and antiresonance ($h\nu_{AR}=47$ eV, dashed line). The zero of the binding-energy scale in Fig. 2 corresponds to the position of the Fermi level E_F in CdTe. Since the different ternary alloy samples exhibited variable doping, we aligned the valence-band maxima of the different EDC's in Fig. 2 with the value of E_v in CdTe to facilitate comparison with the results for the binary. Therefore, the apparent energy difference E_v-E_F for the ternary samples in Fig. 2 is not consistent with the actual doping. The position

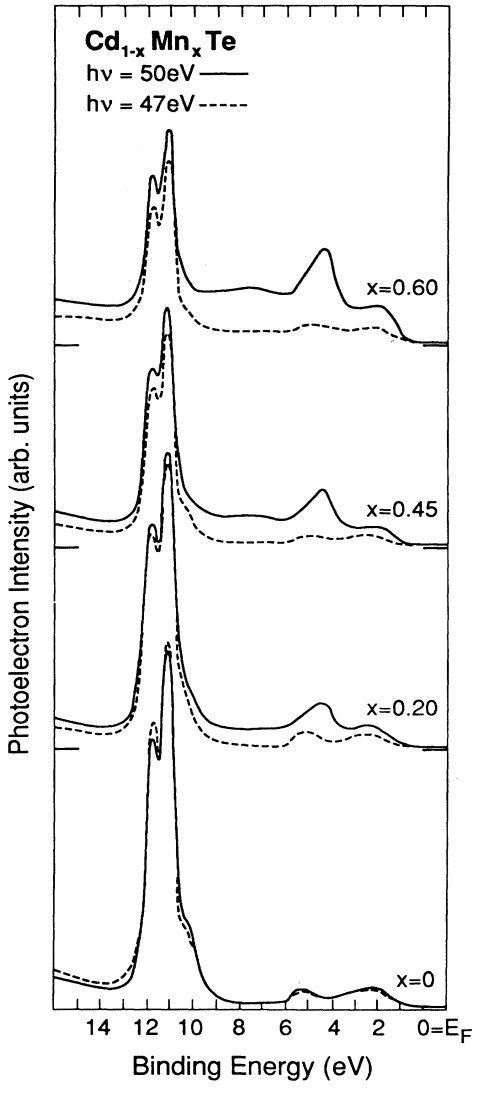

FIG. 2. EDC's for the valence-band and Cd 4*d* emission from $Cd_{1-x}Mn_xTe$ bulk semimagnetic semiconductors cleaved *in situ*. EDC's at resonance ($h\nu_R=50$ eV, solid line) and antiresonance ($h\nu_{AR}=47$ eV, dashed line) emphasize and suppress, respectively, the Mn 3*d* contribution. The Cd 4*d* core intensity (9–13 eV) for each sample was scaled by a $(1-x)$ factor derived from electron-microprobe analysis in order to compare the spectra with those in Fig. 1.

of E_v was estimated through a linear extrapolation of the leading band edge at a photon energy of 47 eV, at which the Mn 3*d* contribution is minimized.[31] The Cd 4*d* integrated intensity for the different samples was normalized[32] to the Cd concentration $(1-x)$ in order to allow direct comparison of the emission intensities in Figs. 1 and 2. In Fig. 1, the EDC's from the Mn-CdTe(110) interface during the first stage of interface formation ($\Theta \leq 3$ Å) appear qualitatively similar to those of the bulk ternary samples in Fig. 2, while they are markedly different from the results for metallic Mn (topmost EDC in Fig. 1). This suggests that $Cd_{1-x}Mn_xTe$-like species may have formed at the Mn-CdTe(110) interface.

To probe atomic interdiffusion across the interface, we analyzed the Cd 4*d* and Te 4*d* core emission as a function of Mn coverage.[32] The integrated intensities of these core levels are plotted in Fig. 3(a). The depth dependence was investigated through comparison of measurements taken at different photon energies.[33] We examined the Cd 4*d* core levels (circles) at $h\nu=40$ and 95 eV, corresponding, respectively, to escape depths $\lambda=4.0\pm0.4$ and 7.6 ± 0.8 Å (Ref. 34), and the Te 4*d* core levels (diamonds) at $h\nu=58$ and 110 eV, corresponding to $\lambda=5.9\pm0.6$ and 6.3 ± 0.6 Å, respectively, from Ref. 34. The hatched region in Fig. 3(a) marks the boundaries of the expected coverage dependence of the core emission, assuming no interdiffusion, layer-by-layer growth, and an escape depth of 4.0–7.6 Å.

In Fig. 3(a) we observe no detectable difference in the core-emission attenuation rate for the different escape depths [Fig. 3(a), open versus solid symbols], so that the measured intensities must reflect relatively uniform sample composition throughout our sampling depth. The Cd 4*d* signal in Fig. 3(a) (circles) decays with Mn coverage at a rate inconsistent with layer-by-layer growth with no interdiffusion. The observed attenuation length [1.5 Å, corresponding to the lower dashed line in Fig. 3(a)] is far shorter than the expected escape depth. We suggest that the surface layer of the semiconductor is partially depleted of Cd as a result of Mn in-diffusion. In this case, the Te- and Mn-derived core emission should exhibit a characteristic coverage dependence. We expect a very slow attenuation of the Te core emission, since Mn would diffuse into the semiconductor rather than simply cover the surface, and a parallel slow rate of increase of the Mn intensity. A coverage dependence of this type has been observed during metal-cation exchange reactions at a number of metal-semiconductor interfaces.[28,35,36]

The attenuation rate of the Te 4*d* emission (diamonds) is indeed much slower than expected from layer-by-layer growth of an unreactive film [hatched area in Fig. 3(a)]. Over 80% of the initial Te signal is still observed at a Mn coverage of 3 Å (3.5 ML). The Te 4*d* attenuation rate would be consistent with the presence of an unreactive interface only if the photoelectron escape depth were approximately 20 Å [see the corresponding upper dashed line in Fig. 3(a)].

Results for the Te 4*d* and Cd 4*d* core line shapes are not presented here for brevity. We mention, though, that the Te 4*d* line shape remains unchanged for $\Theta \leq 1$ Å and exhibits only slight indications of broadening for coverages $\lesssim 3$ Å. An apparent "sharpening" of the Cd 4*d* line shape, as a result of Mn deposition, is consistent with the changes observed in comparing the Cd 4*d* emission in $Cd_{1-x}Mn_xTe$ versus CdTe,[5] and is mostly the result of modification of the Te 5*s* contribution, which is partly su-

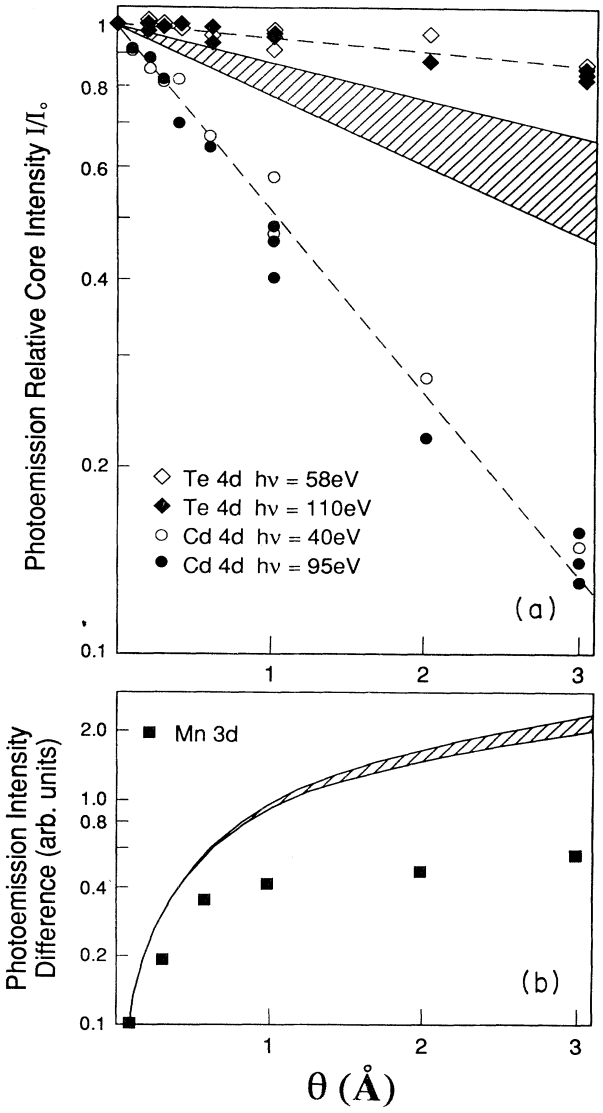

FIG. 3. (a) Integrated intensities for the Te 4*d* and Cd 4*d* core levels as a function of Mn coverage Θ. The relative intensities were measured at different photon energies corresponding to higher (open symbols) or lower (solid symbols) surface sensitivity in bulk CdTe (Ref. 34). The range of attenuation rates expected in the absence of interdiffusion for escape depths between 4.0 and 7.6 Å is shown by the hatched area. Lines drawn through the Cd 4*d* and Te 4*d* data correspond to attenuation lengths of 1.5 and 20 Å, respectively. (b) Intensity of the Mn 3*d* emission as a function of coverage measured from the integrated area of the difference curve between the resonance and antiresonance EDC's of Fig. 1. The range of expected intensities in the absence of interdiffusion is shown by the hatched area. Theoretical and experimental intensity values have been normalized to each other for $\Theta=0.1$ Å.

perimposed to the Cd 4*d* bulk and surface doublets.[5,24]

Atomic interdiffusion at the interface should also result in drastic changes in the Mn emission intensity and line shape relative to those expected for layer-by-layer formation of an unreacted interface. We have already shown in Fig. 1 that the Mn 3*d* line shape for $\Theta < 3$ Å is inconsistent with the presence of unreacted Mn and consistent with the formation of a semimagnetic alloy. As far as the Mn emission intensity is concerned, the only Mn core levels accessible in the photon energy explored were the Mn 3*p* levels, with relatively low cross section. Therefore we elected to use the resonant 3*d* valence emission intensity to gauge the Mn concentration. We calculated resonance-antiresonance difference curves from the EDC's in Figs. 1 and 2 following the methodology proposed in Refs. 3, 5, and 31. The results are illustrated in Fig. 4 for the Mn-CdTe interface, and in Fig. 5 for the bulk ternary samples. In both figures, the dashed line in the 10–13-eV binding-energy range replaces spurious structure due to imperfect cancellation of the Cd 4*d* and Te 5*s* emission.[5] The bulk-alloy difference curves in Fig. 5 are in good agreement with those of Refs. 3 and 5.

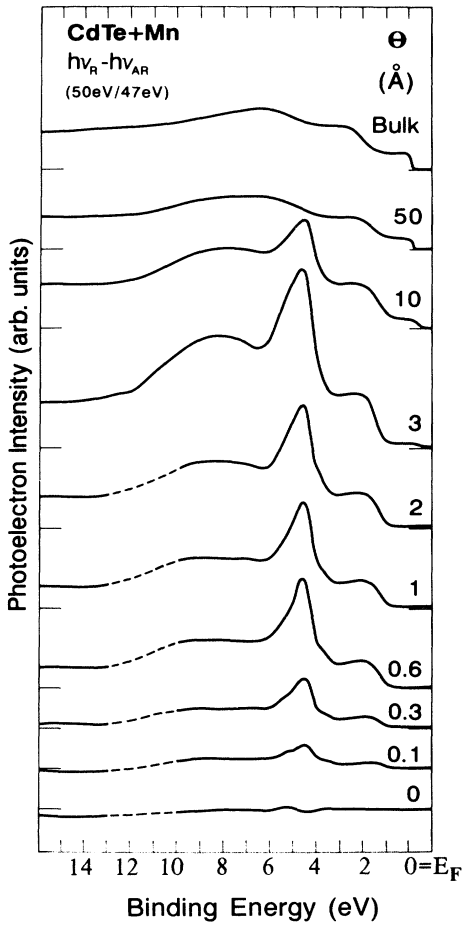

FIG. 4. Resonance-antiresonance difference curves from the Mn-CdTe(110) interface for various Mn coverages. The curves were obtained by subtracting the $h\nu_{AR}=47$ eV data of Fig. 1 from the corresponding $h\nu_R=50$ eV curve at the same Mn coverage. The results emphasize the coverage dependence of the Mn 3*d* contribution. The topmost difference curve was obtained from a thick unreacted Mn film on Si(111).

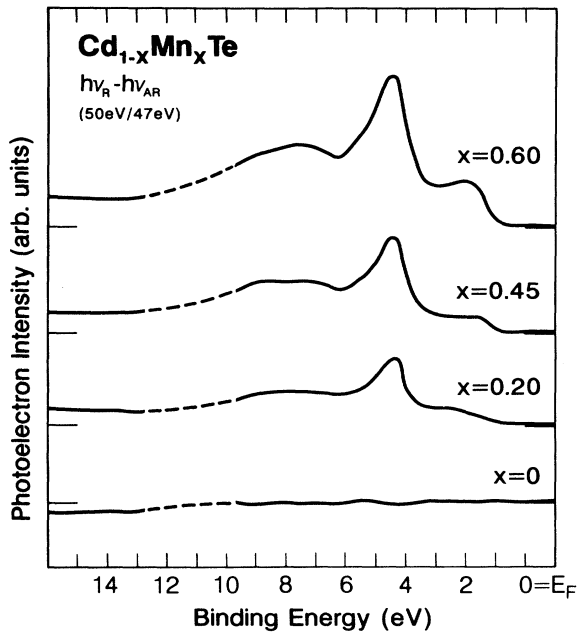

FIG. 5. Resonance-antiresonance difference curves for bulk semimagnetic $Cd_{1-x}Mn_xTe$ semiconductor standards at selected values of x. These curves were obtained from the EDC's in Fig. 2 and represent the Mn 3*d* contribution to the valence-band emission in the bulk ternary alloys.

The Mn integrated emission from the interface and the bulk-alloy spectra has been calculated by integrating the difference curves in Figs. 4 and 5 after subtraction of a linear background interpolated between 0 and 16–17 eV. We emphasize that the background subtraction was performed in an identical manner for bulk and interface difference curves. The interface results are plotted in arbitrary units in Fig. 3(b) as a function of Mn coverage (solid squares). Mn-CdTe intermixing is supported by a comparison of the experimental results in Fig. 3(b) (solid square) with the theoretical trend expected in the absence of interface reaction. In the absence of interdiffusion and island formation, the Mn emission intensity would increase with coverage approximately as

$$I_0/I_f=[1-\exp(-\Theta_0/\lambda)] ,$$

where I_0 is the Mn emission intensity for a coverage Θ_0, and I_f is the emission intensity for a thick Mn film ($\Theta\rightarrow\infty$). In our case, the final line shape at high Mn coverages is radically different, and it is not possible to derive an appropriate value for I_f. We can consider, however, *relative increments* in intensity from a coverage Θ_1 to a coverage Θ_2, and obtain from the previous equation

$$I_2/I_1=\left[\frac{1-\exp(-\Theta_2/\lambda)}{1-\exp(-\Theta_1/\lambda)}\right] ,$$

where the symbols have their obvious meaning. This expression will be applicable only in the coverage range where the Mn 3*d* line shape remains relatively unchanged ($0 < \Theta < 3$ Å). We selected a Mn coverage of 0.1 Å as an arbitrary reference, assumed an escape depth λ of 3–4 Å,[34] and normalized the theoretical curve and the experimental data at the reference coverage. The corresponding expected rate of increase of the Mn emission (for $\Theta > 0.1$ Å) in the absence of interdiffusion is shown by the hatched region in Fig. 3(b). Comparison with experiment shows that the Mn emission increases with coverage at a rate which is only 50–60 % of the theoretical rate. We emphasize that this result is not substantially affected by a different choice of the reference thickness. The low rate of increase in the Mn 3*d* intensity is consistent with the proposed Mn in-diffusion.

Together, the behavior of the Cd 4*d*, Te 4*d*, and Mn 3*d* emission argue compellingly in favor of the formation of a $Cd_{1-x}Mn_xTe$ surface layer,[37] as a result of a partial Mn-Cd exchange reaction. This type of atomic interdiffusion across the interface is likely to yield a composition gradient in the direction normal to the interface. In other words, while the surface region of a cleaved semiconductor is likely to be stoichiometric and reflect the bulk composition, this is not necessarily the case for *reacted* surfaces. However, the lack of escape-depth dependence in the results of Fig. 3 indicates a relatively homogeneous composition of the ternary layer on the scale of the photoemission sampling depth. Only on this basis, and within the limits of such a simplistic assumption, will we define and estimate an average composition $\bar{x}$ of the reacted layer.

B. Semimagnetic surface-layer composition

The composition of the surface layer can be examined using the bulk ternary semiconductor samples as standards. The relative homogeneity of the surface alloy observed in Fig. 3 suggests that an average Mn concentration $\bar{x}$ within the surface layer can be used to characterize the layer properties. We estimated $\bar{x}$ at each Θ from the [Mn]/[Cd] emission intensity ratio in the interface alloy and in the bulk standards. The Mn emission intensity was determined integrating the resonance-antiresonance difference curves as described in the preceding section for the interface results in Fig. 3(b). The Cd intensity was obtained from the integrated Cd 4*d* core emission at $h\nu = 50$ eV (Ref. 32). The resulting [Mn]/[Cd] ratio from the bulk standards is compared in the inset of Fig. 6 (solid triangles) with the expected $x/(1-x)$ dependence (solid line); x was determined from the electron-microprobe analysis. The remarkable agreement indicates that the photoemission [Mn]/[Cd] ratio can be used to gauge the composition of the $Cd_{1-x}Mn_xTe$ interface reaction products.

From the data in Fig. 1 we calculated the [Mn]/[Cd] ratio for the interface, and estimated $\bar{x}$ assuming the ratio proportional to $\bar{x}/(1-\bar{x})$. We plot in Fig. 6 the resulting values of $\bar{x}$ as a function of the metal coverage Θ. In view of the uncertainties involved in the analysis, we estimate the overall accuracy as about 10% of each $\bar{x}$ value

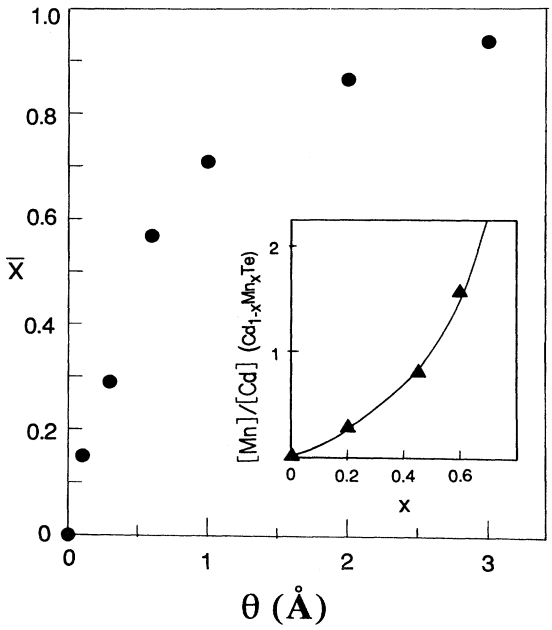

FIG. 6. Average Mn concentration $\bar{x}$ of the $Cd_{1-x}Mn_xTe$ surface alloy formed through Mn-CdTe(110) interface reaction as a function of Mn coverage (circles). In the inset is a plot of the photoemission [Mn 3*d*]/[Cd 4*d*] intensity ratio for selected bulk $Cd_{1-x}Mn_xTe$ samples (triangles) as a function of x. The expected $x/(1-x)$ dependence is shown by a solid line.

in Fig. 6. The highest Mn concentration observed in the $Cd_{1-x}Mn_xTe$ interface reaction products ($\bar{x} = 0.87$ and 0.94 in Fig. 6) would be above those that can be obtained through conventional bulk-crystal growth techniques. However, a word of caution is required here. For $x > 0.77$ in bulk single crystals one observes[10] the presence of a MnTe second phase. On the basis of our photoemission results we cannot rule out the presence of a MnTe second phase at the interface. The results of Fig. 3 suggest a relatively homogeneous composition in the direction perpendicular to the interface on the scale of the photoemission sampling depth, but provide no information on the *lateral* homogeneity of the reaction products. Our estimates for the average composition $\bar{x}$ of the surface alloy have therefore to be intended as an average of the local composition within the sampling depth *and* across the surface.

Emission at E_F is visible in the $\Theta = 3$ Å spectrum in Fig. 4, so that the large $\bar{x}$ value (0.94) determined for this coverage may in principle be affected by the presence of unreacted Mn. To estimate this effect, we subtracted the unreacted Mn contribution using the bulk Mn difference curve in Fig. 4 (topmost spectrum) scaled down to the emission intensity at E_F in the $\Theta = 3$ Å spectrum. The modified [Mn]/[Cd] intensity ratio results in a value of $\bar{x}$ lowered by 6–7 %, so that the Mn atomic concentration in the reacted phase for $\Theta = 3$ Å may be as low as 0.87–0.88, where the smaller of the two values corresponds to the higher estimate of the unreacted Mn contri-

bution. This lower value of $\bar{x}$ would suggest a trend toward saturation in the ternary alloy composition for $2<\Theta<3$ Å. We emphasize that the choice of integration range and background (linearly interpolated between 0 and 16–17 eV) for the Mn $3d$ emission was identical for bulk and interface results, so that it does not affect the comparison of the corresponding Mn concentrations.

We suggest that such high Mn concentrations are achievable at the interface because of the metastable character of the reaction products. Although we describe the $Cd_{1-x}Mn_xTe$ interface reaction products as metastable, we caution the reader that, to our knowledge, the x dependence of the surface free energy of $Cd_{1-x}Mn_xTe$ has never been determined, and we did not perform any study of the temperature dependence of composition and structure of the reaction products.

The reduced escape-depth dependence of the results of Fig. 3 suggest a substantial room-temperature diffusion length for Mn in CdTe, and the consequent formation of a relatively thick $Cd_{1-x}Mn_xTe$ surface layer. A rough estimate of this thickness can be made using the values of $\bar{x}$ in Fig. 6. At a coverage of 2 Å (2.4 ML), $\bar{x}=0.87$ in Fig. 6. If Mn atoms replace 87% of the cations in the semiconductor lattice, then the thickness of the layer in which the exchange reaction has occurred will be 2(2.4 ML)(2.3 Å/ML)/0.87=12.7 Å. For lower coverages Θ, the Mn concentration $\bar{x}$ is smaller, and so will be the estimated layer thickness. For example, at $\Theta=0.1$ Å it is $\bar{x}=0.15$ in Fig. 6, and the corresponding estimated layer thickness is 3.7 Å. Admittedly, such estimates are based on the simplistic assumption of composition homogeneity, and we should at least explore if such an assumption is quantitatively consistent with the lack of escape-depth dependence in the results of Fig. 3. We focus on the Cd $4d$ results for which we have the widest variation in escape depth in Fig. 3. Since Mn is in-diffusing in CdTe, the relevant escape depth is that of photoelectrons in CdTe. Using values of 4.0±0.4 and 7.6±0.8 Å, respectively, for the low- and high-photon-energy results in Fig. 3, we can estimate[38] the expected variation in the Cd $4d$ intensity as a function of coverage given a surface layer of composition $\bar{x}$. We find that the high-photon-energy results are quantitatively consistent (within the scattering of the experimental data of about 20%) with the prediction of our simplistic model. However, the low-photon-energy results are lower than the experimental data by about 1% for $\Theta=0.1$ Å and about 30% for $\Theta=2$ Å, and therefore not strictly consistent with our simplistic assumption. The presence of about 0.06 ML of segregated Cd visible in the high-coverage spectra[25] would be sufficient to explain such a discrepancy. At $\Theta=2$ Å, for the segregated Cd layer on top of a homogeneous ternary layer of composition $\bar{x}=0.87$, the expected residual Cd emission would be 34% of the original emission at $h\nu=95$ eV, and 24% at $h\nu=40$ eV, consistent with the observed results (within an experimental uncertainty of 20%).

We emphasize that the amount of segregated Cd (0.06 ML) visible at high coverages is much less of the total number of Cd atoms displaced during interface reaction. For example, at $\Theta=2$ Å the formation of a 12.7-Å-thick layer of a surface alloy with $\bar{x}=0.87$ would produce about 2 ML of displaced Cd atoms. Most such atoms are not present within the photoemission sampling depth, since their presence would give rise to a much slower Cd $4d$ attenuation rate with Mn coverage than observed and/or dominant metallic Cd $4d$ emission features. We propose that while a small fraction of such atoms remain segregated at the surface, most of them diffuse away from the sampled region. Cd is known to exhibit a large room-temperature diffusion coefficient in II-VI semiconductors,[39] and cation losses due to interface reactions have been observed in other related systems.[40] It is to date a matter of debate if the displaced cations diffuse in the bulk of the semiconductor or escape into vacuum, consistently with the large cation vapor pressure. Our results cannot discriminate between the two behaviors. We mention, however, that recent experiments on interface reactions of related systems under oxide capping layers[41] indicate systematically reduced intermixing at the interface under capping, therefore supporting the second mechanism.

The small initial value of the layer thickness (at small Θ) is probably related to variations in the Mn diffusion length in CdTe. At low Mn coverage, there is a relatively high probability of a Cd-Mn exchange reaction in the first layer of the semiconductor. At higher coverages, most of the Cd atoms in the topmost layers have been replaced by Mn, and the reaction may become diffusion limited. This stage ($\Theta\gtrsim 3$ Å) corresponds to the saturation in the layer composition $\bar{x}$ observed in Fig. 6, and to the appearance of unreacted metallic Mn on top of the ternary layer, as shown by the metallic Fermi level and the evolution of the valence-band emission in Fig. 1. The relatively large values of the layer thickness at $\Theta\sim 2$–3 Å imply substantial room-temperature Mn diffusion lengths in CdTe. Both surface and bulk thermodynamic parameters may therefore play a role in determining the evolution of this interface.

C. Ternary electronic structure

We can use the data of Figs. 1 and 4 to gain information on the composition dependence of the Mn $3d$ contribution to the valence-band structure in $Cd_{1-x}Mn_xTe$. The resonance-antiresonance difference curves for $\Theta\leq 3$ Å in Fig. 4 and for the bulk samples in Fig. 5 emphasize three main Mn-related features, i.e., major structure at 4.35 eV, smaller structure at 1–3 eV, and a broad satellite in the 7–9-eV range.[3,5] The similarity between the results of Figs. 4 and 5 is exemplified in Fig. 7, where we plot the Mn $3d$ valence-band contribution for Mn-CdTe(110) at a coverage of 0.6 Å (solid circles) corresponding to $\bar{x}=0.57$, superimposed to the corresponding result for a cleaved single-crystal sample with $x=0.60$ (open squares). The binding energies in Fig. 7 are referred to the valence-band maximum E_v, and the three $3d$ features appear now at 3.6, 0.3–2.3, and 6.3–8.3 eV, respectively. One-electron density-of-states calculations for a hypothetical zinc-blende MnTe (Refs. 5 and 6), and first-principles or semiempirical calculations for $Cd_{1-x}Mn_xTe$,[7–9] indicate that the 3.6-eV feature

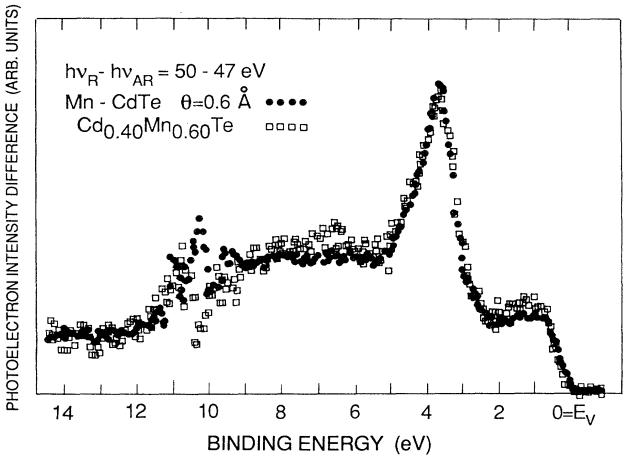

FIG. 7. Comparison of the Mn $3d$ contribution to the valence-band emission (resonance-antiresonance difference curves) from the interface reaction products at $\Theta = 0.6$ Å ($\bar{x} = 0.57$, solid circles) and from a bulk standard ($x = 0.60$, open squares) cleaved *in situ*.

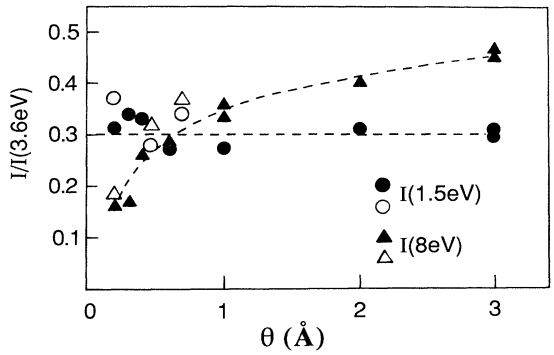

FIG. 8. Photoelectron peak emission intensity from Mn $3d$ states 1.5 eV below the valence-band maximum (solid circles, surface alloys; open circles, bulk ternary alloys) and the satellite 8.0 eV below E_v (solid triangles, surface alloys; open triangles, bulk ternary alloys), relative to the main $3d$ spectral feature 3.6 eV below E_v. All of the data were determined from the peak intensity relative to a secondary background (linearly interpolated between 0 and 16–17 eV) in the resonance curves of Figs. 1 and 2.

is[3–5,7,9] mostly of e_g symmetry (Γ_{12}), and remains relatively unhybridized, exhibiting the strongest resonant enhancement.[5] The t_{2g} states, on the other hand, mix with Te p-derived orbitals of the same symmetry (Γ_{15}), and the resulting hybrid states account for the Mn $3d$ contribution in the 1–2-eV range in the resonance-antiresonance curves. Trends in the relative intensity of the first two features in the ternary semimagnetic semiconductor series should reflect the Mn d–anion p relative degree of mixing.[3,5]

The broad emission feature 6–8 eV below E_v does not appear in one-electron ground-state calculations, and has been associated by Fujimori and co-workers[3] with a many-electron satellite.[31,43–47] In the configuration-interaction calculation for a model $MnTe_4^{6-}$ cluster of Ref. 3 the satellite is associated with an unscreened d^4 final state, while the other two Mn $3d$ features reportedly both correspond to a d^5L final-state configuration. In this configuration, the core hole is fully screened through charge transfer from a Te p-derived ligand orbital. The results of the calculations[3] are in good agreement with the photoemission resonance-antiresonance difference curves, but the model contains several fitting parameters (energy difference between the final-state configurations; lifetime of each configuration) that are determined through comparison with the experimental EDC's. In our opinion, the validity of the model can be judged only from the accuracy of its predictions about the *character* of the different Mn-derived spectral features.

The evident changes with composition $\bar{x}$ of the Mn $3d$ signature in Fig. 4 suggest that the concentration dependence of the different Mn features should be examined in the light of the cluster-model versus one-electron picture. For $\Theta \leq 3$ Å it appears that the relative intensity of the states within 3 eV of E_v increases with coverage at a rate similar to that of the main structure 3.6 eV below E_v. The emission intensity (relative to a linear background) 1.5 eV below E_v remains about 30% of the main line for all coverages $0.2 < \Theta < 3$ Å ($0.29 < \bar{x} < 0.94$). The intensity ratio $[I(1.5\text{ eV})]/[I(3.6\text{ eV})]$ is plotted (solid circles) as a function of Mn coverage in Fig. 8. The corresponding ratio for the bulk ternary samples is also plotted (open circles) in Fig. 8 for comparison.[48] Along the same lines, we have also calculated the ratio of the satellite emission relative to the main line as a function of Θ, using the peak emission intensity relative to a linear background at initial energies of 8.0 eV (satellite) and 3.6 eV (main line) below E_v. The $[I(8.0\text{ eV})/[I(3.6\text{ eV})]$ ratio is also plotted in Fig. 8 (solid triangles). The open triangles show the corresponding ratios in the bulk ternary samples.[48] For coverages $\Theta \leq 3$ Å, the relative satellite intensity is approximately proportional to the Mn concentration $\bar{x}$: $[I(8.0\text{ eV})]/[I(3.6\text{ eV})] = C\bar{x}$, where $C = 0.5 \pm 0.05$.

The results in Fig. 8 indicate that there is a large concentration dependence of the satellite intensity, while the $3d$-related DOS features all exhibit the same behavior with composition. The latter result is consistent with both the predictions of the one-electron calculations and the cluster model, since the Mn-Te coordination remains largely unchanged as a function of the Mn concentration[42] in the alloy. The variation of the relative intensity of the satellite with x is instead an unexpected result. An increase in x in the alloy has two main effects: an increase in the fundamental band gap, and an increase in the d-d second-nearest-neighbor interaction. If the satellite corresponds to an unscreened d^4 final state, as proposed by the cluster model, the change in band gap and d-d interaction should leave it relatively unaffected. The observed concentration dependence therefore indicates that the proposed identification of the many-body final state which accounts for the satellite feature (d^4 unscreened final state) should be reexamined.

IV. CONCLUSIONS

We have shown that deposition of Mn onto CdTe(110) surfaces at room temperature yields interdiffusion across the interface and the formation of nonequilibrium $Cd_{1-x}Mn_xTe$ surface alloys, where x varies with the Mn coverage Θ. An estimate of the average concentration $\bar{x}$ within the surface layer was performed using core-level intensity ratios and data for bulk ternary standards. The results suggest a relatively homogeneous composition of the surface layer, and surprisingly large Mn diffusion lengths in CdTe at room temperature.

The interface data were used to examine the composition dependence of the Mn contribution to the electronic structure of semimagnetic semiconductors. The results indicate that the level of Mn d–Te p hybridization is independent of x, as expected, but that the relative intensity of the $3d$ many-body satellite is concentration dependent and increases linearly with $\bar{x}$. We conclude that the proposed unscreened d^4 identification of the many-body final state responsible for the satellite should be reexamined.

ACKNOWLEDGMENTS

This work was supported by the Office of Naval Research of the U.S. Department of Defense under Grant No. N00014-89-J-1407, and by the Center for Interfacial Engineering at the University of Minnesota. We thank J. K. Furdyna for providing us with the bulk crystals used in the present study and for encouragement and support. We are indebted to a number of colleagues for comments and for providing us with results of their work prior to publication: A. Balzarotti, M. De Crescenzi, J. D. Dow, L. Ley, C. Mailhiot, and K. C. Prince. Finally, we would like to express our appreciation to the entire staff of the University of Wisconsin–Madison Synchrotron Radiation Center (supported by the National Science Foundation) for their support.

[1]A. Franciosi, in *Diluted Magnetic (Semimagnetic) Semiconductors,* edited by R. L. Aggarwall, J. K. Furdyna, and S. von Molnar (Materials Research Society, Pittsburgh, 1987), p. 175, and references therein.

[2]A. Wall, C. Caprile, A. Franciosi, R. Reifenberger, and U. Debska, J. Vac. Sci. Technol. A **4**, 818 (1986); A. Wall, C. Caprile, A. Franciosi, M. Vaziri, R. Reifenberger, and J. K. Furdyna, *ibid.* **4**, 2010 (1986); A. Wall, S. Chang, P. Philip, C. Caprile, A. Franciosi, R. Reifenberger, and F. Pool, *ibid.* **5**, 2051 (1987).

[3]L. Ley, M. Taniguchi, J. Ghijsen, R. L. Johnson, and A. Fujimori, Phys. Rev. B **35**, 2839 (1987); M. Taniguchi, M. Fujimori, M. Fujisawa, T. Mori, I. Souma, and Y. Oka, Solid State Commun. **62**, 431 (1987).

[4]V. Chab, K. C. Prince, M. Surman, and A. M. Bradshaw, Phys. Rev. B **38**, 12 353 (1988).

[5]A. Wall, A. Franciosi, Y. Gao, J. H. Weaver, H.-H. Tsai, J. D. Dow, and R. V. Kasowski, J. Vac. Sci. Technol. A **7**, 656 (1989); A. Franciosi, A. Wall, Y. Gao, J. H. Weaver, M.-H. Tsai, J. D. Dow, R. Reifenberger, and F. Pool, Phys. Rev. B **40**, 12 009 (1989).

[6]M.-H. Tsai, J. D. Dow, R. V. Kasowski, A. Wall, and A. Franciosi, Solid State Commun. **69**, 1131 (1989).

[7]B. E. Larson, K. C. Hass, H. Ehrenreich, and A. E. Carlsson, Solid State Commun. **56**, 347 (1985); H. Ehrenreich, K. C. Hass, N. F. Johnson, B. E. Larson, and R. J. Lempert, in *Proceedings of the 18th International Conference on the Physics of Semiconductors,* edited by O. Engström (World Scientific, Singapore, 1987), pp. 1751–1754.

[8]S.-H. Wei and Z. Zunger, Phys. Rev. B **35**, 2340 (1987); Phys. Rev. Lett. **56**, 2391 (1986).

[9]K. C. Hass and H. Ehrenreich, J. Cryst. Growth (to be published).

[10]J. K. Furdyna, J. Vac. Sci. Technol. A **4**, 2002 (1986).

[11]N. B. Brandt and V. V. Moshchalkov, Adv. Phys. **33**, 193 (1984).

[12]M. Podgorny, Z. Phys. B **69**, 501 (1988).

[13]J. Masek, B. Velicky, and V. Janis, Acta Phys. Polon. A **69**, 1107 (1986).

[14]Such average compositions are obtained from the Mn-to-Cd integrated-photoemission-intensity ratio as described in the text. At the highest values of $\bar{x}$, the presence of some unreacted metallic Mn may cause discrepancies of up to 6–7 % between the calculated value of $\bar{x}$ and the actual composition of the ternary reacted phase. Even a maximum Mn concentration of only 0.87 (rather than 0.94) in the ternary would exceed the maximum concentration attainable through bulk-crystal growth methods, but on the basis of photoemission results above it is not possible to rule out the presence of a MnTe second phase for $\bar{x} > 0.77$.

[15]U. Fano, Phys. Rev. **124**, 1866 (1961).

[16]L. C. Davis and L. A. Feldkamp, Phys. Rev. B **23**, 6239 (1981); **17**, 2012 (1978).

[17]Y. Yafet, Phys. Rev. B **21**, 5023 (1980).

[18]Upon deposition of $\Theta > 20$ Å of Mn on Si(111) the valence-band emission converges to a bulklike Mn $3d$ emission, and no Si $2p$ emission could be detected within experimental uncertainty.

[19]A. Wall, Y. Gao, A. Raisanen, A. Franciosi, and J. R. Chelikowsky, Phys. Rev. B **43**, 4988 (1991).

[20]N. J. Shevchik, J. Tejeda, M. Cardona, and D. W. Langer, Phys. Status Solidi B **59**, 87 (1973).

[21]D. E. Eastman, W. D. Grobman, J. L. Freeof, and M. Erbudak, Phys. Rev. B **9**, 3473 (1974).

[22]L. Ley, R. A. Pollak, F. R. McFeely, S. P. Kowalczyk, and D. A. Shirley, Phys. Rev. B **9**, 600 (1974).

[23]J. R. Chelikowsky and M. L. Cohen, Phys. Rev. B **14**, 556 (1976).

[24]K. C. Prince, G. Paolucci, V. Chab, M. Surman, and A. M. Bradshaw, Surf. Sci. **206**, L871 (1988).

[25]At $\Theta = 50$ Å the metallic Mn-like valence-band emission and the large ($\sim$0.9 eV) shift to low binding energy of the residual Cd $4d$ core emission relative to the Cd $4d$ emission in CdTe suggest that a relatively small amount of Cd appears in a Mn-Cd intermetallic phase or as "free" Cd segregated at the film surface. An estimate of the amount of segregated Cd can be made considering that at $\Theta = 50$ Å the residual Cd $4d$ emission intensity is 7% ($h\nu = 40$ eV) of the original emission

intensity. Using the Cd atomic spatial density in CdTe and metallic Cd, and a photoelectron escape depth of 4 Å, the residual 7% Cd intensity is consistent with the presence of 0.06 ML of segregated metallic Cd at the surface.

[26]P. John, T. Miller, T. C. Hsieh, A. P. Shapiro, A. L. Wacha, and T.-C. Chiang, Phys. Rev. B **34**, 6704 (1986).

[27]G. Margaritondo, L. J. Brillson, and N. G. Stoffel, Solid State Commun. **35**, 277 (1980); L. J. Brillson, Phys. Rev. B **31**, 7915 (1985).

[28]L. J. Brillson, Surf. Sci. Rep. **2**, 123 (1982).

[29]J. E. Demuth, W. J. Thompson, N. J. DiNardo, and R. Imbihl, Phys. Rev. Lett. **56**, 1408 (1986).

[30]*Photoemission in Solids II,* edited by L. Ley and M. Cardona (Springer-Verlag, New York, 1979).

[31]A. Wall, A. Franciosi, D. W. Niles, R. Reifenberger, C. Quaresima, M. Capozi, and P. Perfetti, Phys. Rev. B **41**, 5969 (1990). At photon energies near the resonance, the linearly extrapolated value of E_v may appear composition and photon-energy dependent, and may not reflect an actual change in the one-electron density of states because of final-state effects.

[32]After subtraction of the secondary-electron background.

[33]*Photoemission in Solids I,* edited by M. Cardona and L. Ley (Springer-Verlag, New York, 1978).

[34]The corresponding photoelectron escape depths were estimated from the analysis performed in Ref. 19 of the photon-energy dependence of the relative intensity of the Cd 4*d* surface- and bulk-related doublets (see also Refs. 24 and 26). For photoelectrons from the Cd 4*d* core levels we estimate escape depths of 4.0±0.4 and 7.6±0.8 Å, respectively, at photon energies of 40 and 95 eV. For photoelectrons from the Te 4*d* core levels we estimate escape depths of 5.9±0.6 and 6.3±0.6 Å, respectively, at photon energies of 58 and 110 eV. For the major Mn 3*d* valence-band emission feature at resonance, we estimate an escape depth of 3–4 Å.

[35]G. Margaritondo and A. Franciosi, Annu. Rev. Mater. Sci. **14**, 67 (1984).

[36]See, for example, A. Wall, A. Raisanen, S. Chang, P. Philip, N. Troullier, A. Franciosi, and D. J. Peterman, J. Vac. Sci. Technol. A **5**, 3193 (1987), and references therein.

[37]Segregation of Te at the surface of an unreacted Mn film would also be consistent with the observed dependence of the Mn, Cd, and Te emission intensities, but would be inconsistent with the lack of an escape-depth dependence of the results, with the alloy-type valence-band emission in Fig. 1, with the line-shape changes observed for the Cd 4*d* core levels, and with the lack of a modification of the Te 4*d* line shape. Island growth of an unreacted Mn film could explain the low rate of increase of the Mn signal and the reduced escape-depth sensitivity of the results, but would be inconsistent with the behavior of the Cd 4*d* and Te 4*d* attenuation rates, and with the changes in the valence-band emission as a function of Mn coverage observed in Fig. 1.

[38]Assuming a homogeneous Mn concentration x in a ternary layer of thickness d at the surface of CdTe, the intensity $I(\Theta)$ of the Cd 4*d* emission should decrease with coverage Θ as $I(\Theta)=I(0)[(1-x)+\exp(-d/\lambda)x]$, where $I(0)$ is the initial Cd 4*d* emission intensity prior to Mn deposition, and λ is the photoelectron escape depth.

[39]Y. Kim, A. Ourmazd, and R. D. Feldman, J. Vac. Sci. Technol. A **8**, 1116 (1990).

[40]D. J. Friedman, G. P. Carey, J. Lindau, and W. E. Spicer, Phys. Rev. B **35**, 1188 (1987).

[41]T. Piotrowski, E. Kaminska, A. Piotrowska, A. Jedrzejczak, and A. Turos, Acta Phys. Polon. A **75**, 177 (1989).

[42]Extended x-ray-absorption fine-structure studies have also shown that Mn-Te nearest-neighbor distances remain largely unchanged in the alloy as a function of x, so the lack of long-range order in the interface reaction products should not cause large changes in the DOS, which mostly reflects the local MnTe coordination. See A. Balzarotti, N. Motta, A. Kisiel, M. Zimnal-Starnawska, M. T. Czyżyk, and M. Podgorny, Phys. Rev. B **31**, 7526 (1985); P. Letardi, N. Motta, and A. Balzarotti, J. Phys. C (to be published).

[43]D. E. Eastman and J. L. Freeouf, Phys. Rev. Lett. **34**, 395 (1975).

[44]G. K. Wertheim and S. Hüfner, Phys. Rev. Lett. **28**, 1028 (1972).

[45]A. Kakizaki and T. Ishii, J. Phys. Soc. Jpn. **55**, 4139 (1986); A. Kakizaki, K. Sugeno, T. Ishii, H. Sugawara, I. Nagakura, and S. Shin, Phys. Rev. B **28**, 1026 (1983).

[46]T. Ishii, S. Kono, S. Suzuki, I. Nagakura, T. Sagawa, R. Kato, M. Watanabe, and S. Sato, Phys. Rev. B **12**, 4320 (1975).

[47]A. Kazikaki, T. Miya, K. Naito, I. Fukui, H. Sugawara, I. Nagakura, and T. Ishii, J. Phys. Soc. Jpn. **54**, 3638 (1985). However, the authors of Refs. 45–47 reverse the t_{2g}-e_g identification of the two 3*d*-derived DOS features.

[48]To incorporate the bulk ternary ratios in Fig. 8, we used the nominal bulk composition x and the calibration in Fig. 6 to obtain equivalent coverages Θ corresponding to the bulk samples.